Spectroscopic investigation of proton bonding at subkelvin temperatures

América Y. Torres-Boy,[a] Martín I. Taccone[a], Katja Ober[a], Myles B. T. Osenton,[a] Gerard Meijer[a], Gert von Helden*[a] and Bruno Martínez-Haya*[b]

[a] *Fritz Haber Institute of the Max Planck Society, 14195 Berlin, Germany; E-mail: helden@fhi-berlin.mpg.de*
[b] *Center for Nanoscience and Sustainable Technologies (CNATS), Universidad Pablo de Olavide, 41013 Seville, Spain; E-mail: bmarhay@upo.es*

Contents

1 Additional Experimental Data

1.1 Mass spectra of the ionic species

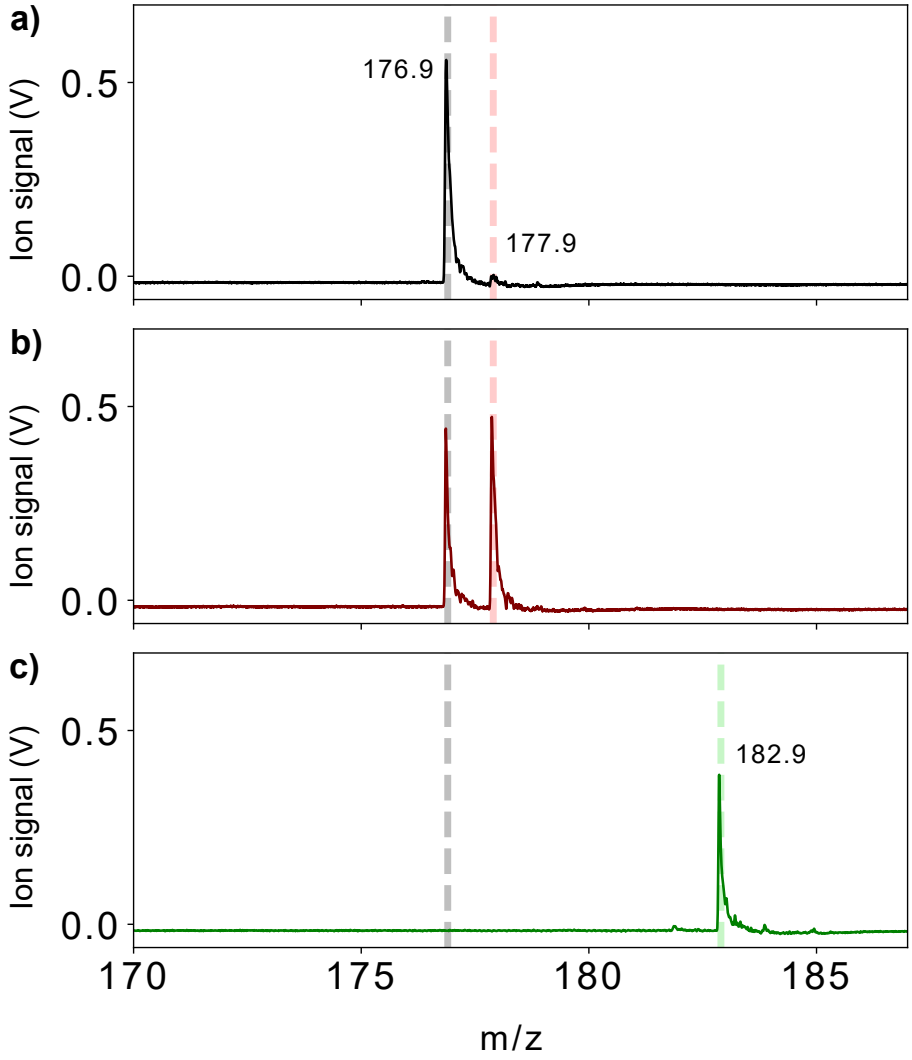

Fig. S1: Time of Flight mass spectra obtained after quadrupole mass separation and prior to injection into the ion trap. **a)** The 12c4-H^+ cation (176.9) with a minor contribution from the ^{13}C isotope (177.9) **b)** The 12c4-H^+ cation (176.9) isolated simultaneously as the 12c4-D^+ (177.9) cation. Here, the resolution of the quadrupole mass filter is lowered to inject both isotopologues with similar abundances into the trap to allow for the simultaneous recording of the IR spectra. **c)** The isolated 12c4-Li^+ cation (182.9).

1.2 List of transitions observed in the IR spectra of 12c4-H$^+$ and 12c4-D$^+$

Table S1: Experimental wavenumbers (cm^{-1}) of the main peaks observed in the He droplet spectra of the 12c4H$^+$ (left column) and 12c4D$^+$ (right column) complexes (see Fig. 3). Greek letters indicate peaks presumably associated with neat vibrational modes of the proton bond.

12c4·H$^+$		12c4·D$^+$	
peak	wavenumber	peak	wavenumber
α	1499.3	a'	1481.24
β	1381.4	b'	1375.3
c	1303.5	c'	1302.4
d	1190.6, 1181.6, 1176.6	d'	1174.5
e	1155.6	e'	1150.5
f	1092.7		
g	1045.8	g'	1044.6
		α'	1029.6
h	991.8	h'	985.6
i	969.8		
j	900.9	j'	884.7
k	839.0		
l	717.8		
m	694.8	m'	604.9
n	662.9		
o	506.0		

1.3 IR spectra of the 12c4-H^+ and 12c4-D^+ at low macropulse energies

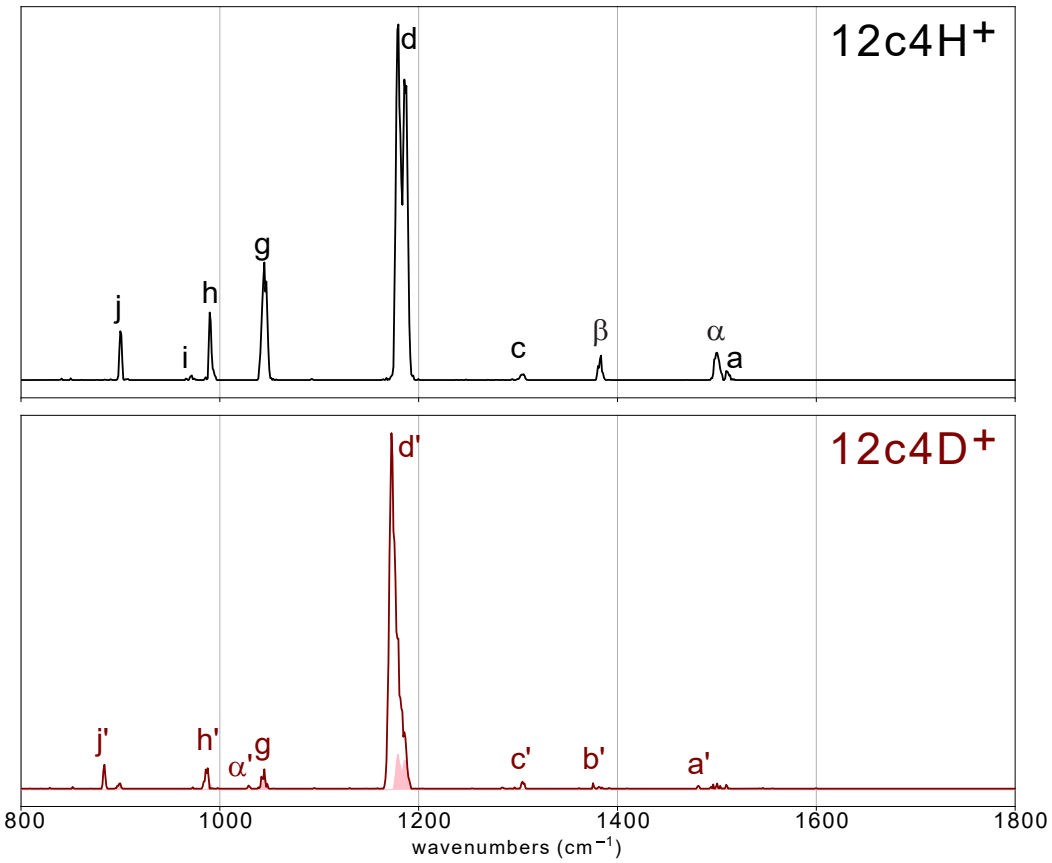

Fig. S2: He droplet IR spectra of the protonated isotopologues 12c4-H^+ (top) and 12c4-D^+ (bottom), recorded at m/z 177 and 178, respectively, using low FEL macropulse energies (∼20 mJ). The shaded curve along the 12c4-D^+ spectrum corresponds to the signal of the ^{13}C isotope of 12c4-H^+ on the m/z = 178 mass channel. Greek letters indicate peaks presumably associated with neat vibrational modes of the proton bond. Due to the highly non-linear nature of the experiment, recording the spectra using low FEL macropulse energies prevents spectral saturation and shows a more realistic relative intensity of the bands.

2 12-crown-4-ether conformers

Density Functional Theory (DFT) and Møller–Plesset perturbation theory (MP2) were employed to model the conformational structure and vibrational signatures of the ions. The basis set aug-cc-pVTZ was employed throughout the study. For DFT, several hybrid and double-hybrid functionals were explored, namely B3LYP, ωB97xD, B2PLYP, DSD-PBEP86 and PBEQIDH, in all cases with Grimme's D3(BJ) dispersion correction[1].

2.1 Structures and energies calculated at different levels of theory

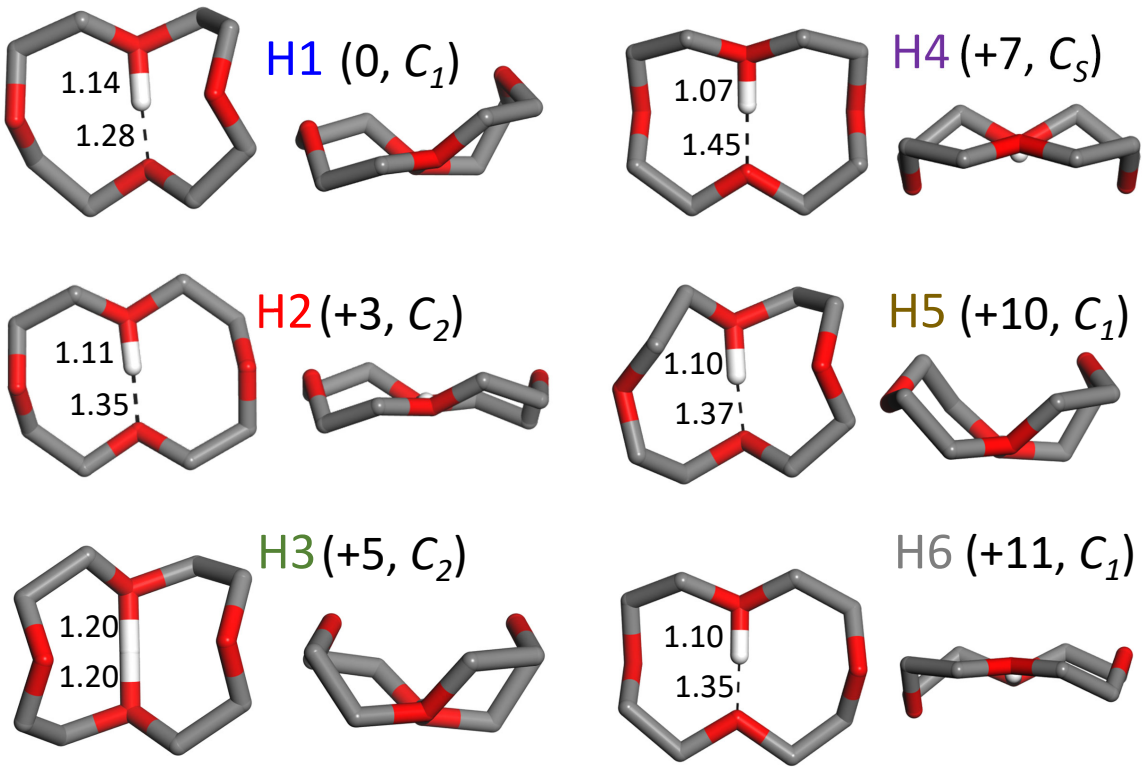

Fig. S3: Schematic representation of the six conformers of lowest energy of the 12c4-H^+ protonated crown ether, H1–H6 (side and top views are depicted with the H atoms of the methylene groups obviated). The corresponding point symmetries of the 12c4 backbone (proton excluded) are indicated along with MP2/aug-cc-pVTZ values of the relative zero-point corrected energies (kJ·mol^{-1}) and the O-H^+ distances (Å). Relative energies of the conformers at different computational levels are provided in Table S2.

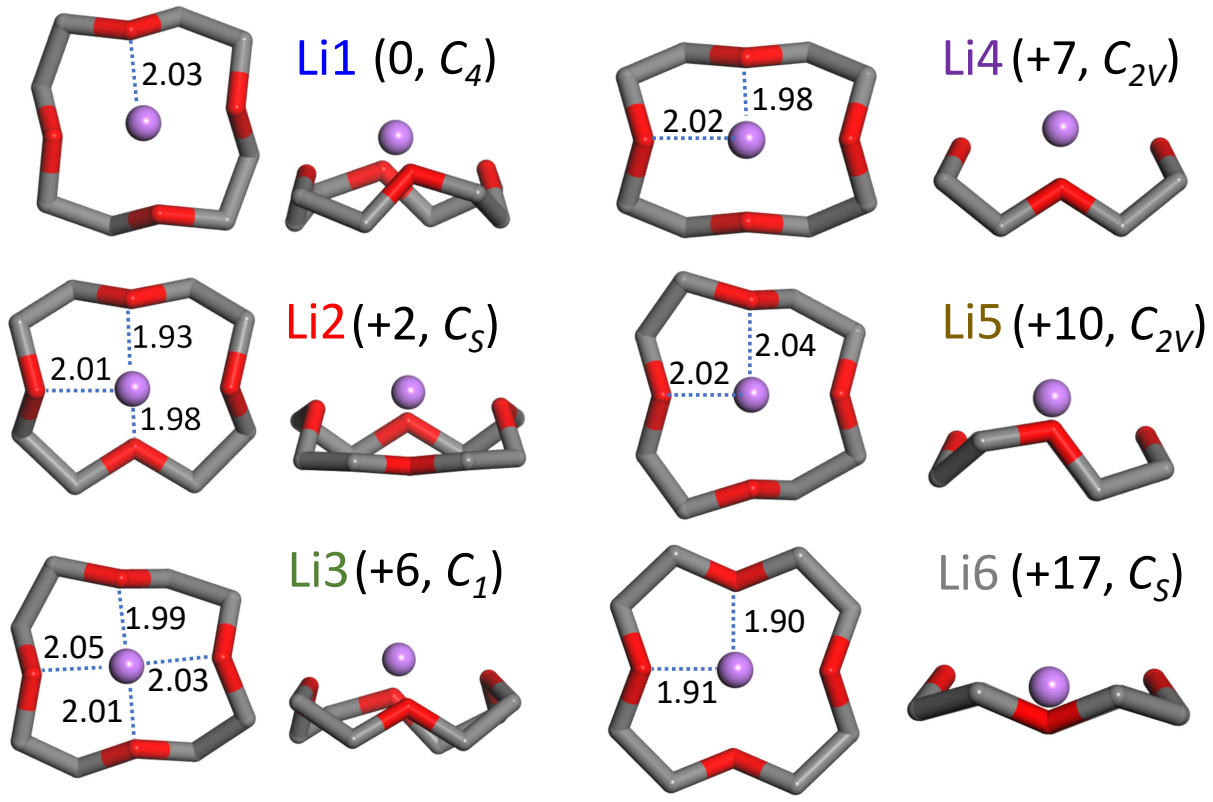

Fig. S4: Schematic representation of the six conformers of lowest energy of the 12c4-Li^+ complex, Li1–Li4 (side and top views are depicted with the H atoms of the methylene groups obviated). The corresponding point symmetries are indicated along with MP2/aug-cc-pVTZ values of the relative zero-point corrected energies (kJ·mol^{-1}) and the O-Li^+ distances (Å).

Table S2. Zero-point corrected electronic energies (in kJ·mol^{-1}) for low-energy conformers of the ions 12c4-Li^+ and 12c4-H^+ (12c4-D^+ in parentheses), at different levels of theory with the basis set aug-cc-pVTZ. The D3(BJ) dispersion correction is applied to all DFT computations

12c4-Li^+				12c4-H^+ (12c4-D^+)						
conf.	MP2	B3LYP	ωB97xD	conf.	MP2	B3LYP	ωB97xD	B2PLYP	DSD-PBEP86	PBE-QIDH
Li1	0.0	0.0	0.0	**H1**	0.0	0.0	0.0	0.0	0.0	0.0
Li2	2.2	0.0	-0.8	**H2**	2.9 (2.6)	-1.2 (-1.5)	0.2 (-0.1)	-0.1 (-0.5)	1.3 (0.8)	-0.2 (0.5)
Li3	6.0	4.5	5.1	**H3**	4.9 (5.2)	3.4 (4.4)	2.2 (3.6)	3.8 (5.1)	4.1 (4.9)	4.9 (5.8)
Li4	7.2	2.9	4.4	**H4**	6.7 (5.5)	7.8 (6.9)	7.0 (6.1)	6.9 (6.0)	6.2 (5.1)	6.4 (5.1)
Li5	10.2	7.9	8.6	**H5**	9.9 (9.1)	7.8 (7.3)	7.6 (7.3)	8.4 (8.0)	9.0 (8.3)	9.1 (7.8)
Li6	16.8	5.9	6.1	**H6**	10.8 (10.0)	7.8 (7.2)	8.3 (7.9)	7.9 (7.6)	8.7 (8.0)	8.5 (7.6)

2.2 XYZ Coordinates for the Optimised Low Energy Geometries

Table S3:Atomic coordinates (in Å) of the six conformers of lowest-enery of protonated 12-crown-4, computed at the MP2/aug-cc-pVTZ level.

	H1			**H2**			**H3**		
O	-0.1413	1.3243	0.4479	-2.4449	0.3086	-0.4731	-0.4278	1.1163	0.8155
O	-2.2084	-0.1930	-0.7183	-0.1894	-1.2218	0.2665	-1.6566	-0.4735	-0.9750
O	0.0314	-1.0676	0.6865	2.4127	-0.2960	-0.4869	0.4277	-1.1163	0.8155
O	1.9511	0.0342	-0.8629	0.1860	1.1918	0.2222	1.6566	0.4735	-0.9750
C	2.1560	1.2807	-0.2017	-0.9947	2.0329	0.2474	1.5531	1.7435	-0.3396
C	0.8678	2.0545	-0.2920	-2.1818	1.1879	0.6146	0.0854	2.0485	-0.1775
C	-1.4934	1.8291	0.2809	-2.5559	-1.0662	-0.1599	-1.8722	1.0121	0.9362
C	-2.4461	0.6673	0.3909	-1.2823	-1.7750	-0.5387	-2.4975	0.4783	-0.3508
C	-2.0161	-1.5664	-0.4239	1.0239	-2.0484	0.2459	-1.5531	-1.7435	-0.3395
C	-0.5389	-1.8773	-0.3897	2.2000	-1.1835	0.5976	-0.0854	-2.0485	-0.1775
C	1.4158	-1.3531	1.0453	2.5466	1.0799	-0.1561	1.8722	-1.0121	0.9362
C	2.3438	-1.1152	-0.1377	1.2744	1.8022	-0.5136	2.4975	-0.4783	-0.3508
H	2.4466	1.1405	0.8422	-1.1397	2.4610	-0.7456	2.0539	1.7547	0.6323
H	2.9476	1.8383	-0.7053	-0.8267	2.8266	0.9760	2.0109	2.5071	-0.9711
H	0.5459	2.1310	-1.3313	-3.0436	1.8378	0.7785	-0.4321	1.8892	-1.1219
H	0.9648	3.0471	0.1481	-1.9867	0.6333	1.5362	-0.0869	3.0552	0.2010
H	-1.5703	2.2764	-0.7101	-3.3694	-1.4894	-0.7509	-2.2676	1.9908	1.2051
H	-1.6758	2.5803	1.0486	-2.7819	-1.2200	0.8974	-2.0119	0.3344	1.7759
H	-3.4697	1.0460	0.3548	-1.3275	-2.8372	-0.3035	-2.6286	1.2708	-1.0842
H	-2.3066	0.1423	1.3393	-1.0335	-1.6256	-1.5889	-3.4863	0.0722	-0.1178
H	-2.4742	-2.1487	-1.2235	1.1373	-2.4490	-0.7608	-2.0109	-2.5071	-0.9711
H	-2.4895	-1.8409	0.5211	0.8615	-2.8476	0.9662	-2.0539	-1.7547	0.6323
H	-0.0545	-1.5981	-1.3241	2.0141	-0.6447	1.5301	0.4321	-1.8892	-1.1219
H	-0.3459	-2.9204	-0.1416	3.0717	-1.8272	0.7383	0.0869	-3.0552	0.2010
H	1.4597	-2.3802	1.4035	3.3684	1.4941	-0.7404	2.2676	-1.9908	1.2051
H	1.6119	-0.6793	1.8762	2.7760	1.2065	0.9037	2.0119	-0.3344	1.7759
H	2.2954	-1.9389	-0.8469	1.0598	1.7246	-1.5806	2.6286	-1.2708	-1.0842
H	3.3721	-1.0467	0.2296	1.3325	2.8526	-0.2246	3.4863	-0.0722	-0.1178
H	-0.0530	0.0503	0.4610	-0.0072	-0.1358	0.1174	0.0000	0.0000	0.6934

Table S3: continued

	H4			**H5**			**H6**		
O	2.2424	0.0367	-0.7814	0.4457	-1.0876	0.8793	0.0047	1.1869	-0.2686
O	0.0003	-1.2688	-0.1376	1.6550	0.4655	-0.9651	-2.2823	0.1243	0.7389
O	-2.2423	0.0362	-0.7814	-0.4981	1.1511	0.6897	-0.0113	-1.2345	0.1817
O	-0.0003	1.1836	0.3232	-2.1388	-1.0268	-0.1139	2.5694	0.0607	-0.3145
C	1.1938	1.9596	0.0797	-1.0880	-1.4931	-0.9452	1.1901	1.9859	-0.0483
C	2.3787	1.0430	0.2180	-0.0356	-2.1112	-0.0611	-1.2140	1.9611	-0.2580
C	2.3888	-1.2936	-0.3328	1.8884	-0.9143	1.0139	-2.3699	1.0050	-0.3759
C	1.2253	-1.7017	0.5484	2.5055	-0.4485	-0.2996	-2.4096	-1.2502	0.4445
C	-1.2246	-1.7018	0.5485	1.5519	1.7568	-0.3656	-1.2557	-1.7519	-0.4002
C	-2.3883	-1.2942	-0.3327	0.0880	2.0857	-0.2438	1.1775	-1.8877	-0.3919
C	-2.3791	1.0425	0.2180	-1.9486	1.1968	0.7469	2.4189	-1.2547	0.1786
C	-1.1945	1.9594	0.0798	-2.5568	0.3160	-0.3213	2.2456	1.1173	0.5805
H	1.2364	2.7763	0.8025	-1.4583	-2.2626	-1.6276	0.9391	2.8110	0.6206
H	1.1481	2.3627	-0.9337	-0.6502	-0.6843	-1.5345	-1.2705	2.5006	0.6886
H	3.2996	1.6050	0.0531	0.8092	-2.4743	-0.6417	-1.1924	2.6671	-1.0896
H	2.4154	0.6131	1.2220	-0.4454	-2.9046	0.5581	1.5208	2.3773	-1.0101
H	3.3196	-1.4503	0.2213	2.3040	-1.8599	1.3561	-2.3261	0.4657	-1.3250
H	2.4081	-1.9062	-1.2313	1.9842	-0.1774	1.8079	-3.3096	1.5594	-0.3434
H	1.1622	-2.7817	0.6582	2.6431	-1.2765	-0.9917	-3.3441	-1.4828	-0.0765
H	1.2322	-1.2276	1.5303	3.4916	-0.0234	-0.0893	-2.4125	-1.7544	1.4082
H	-1.2316	-1.2277	1.5303	2.0405	2.4961	-1.0026	-1.1920	-2.8376	-0.3705
H	-1.1613	-2.7819	0.6584	2.0277	1.7812	0.6178	-1.2911	-1.4193	-1.4375
H	-2.4074	-1.9068	-1.2312	-0.3987	1.9897	-1.2159	1.1401	-1.7669	-1.4746
H	-3.3190	-1.4511	0.2214	-0.0604	3.0935	0.1458	1.0971	-2.9373	-0.1157
H	-2.4159	0.6126	1.2220	-2.2655	2.2363	0.6551	2.3974	-1.2794	1.2707
H	-3.3002	1.6042	0.0529	-2.2109	0.8222	1.7338	3.2713	-1.8470	-0.1589
H	-1.1488	2.3625	-0.9337	-2.2955	0.6546	-1.3267	3.1362	1.7205	0.7672
H	-1.2373	2.7760	0.8025	-3.6427	0.3478	-0.2271	1.8871	0.7250	1.5361
H	0.0003	-0.1969	-0.1263	-0.0123	-0.1039	0.7168	0.0072	-0.1493	0.0341

Table S4: Atomic coordinates (in Å) of the four conformers of lowest-enery of the complex (12-crown-4)-Li^+, computed at the MP2/aug-cc-pVTZ level

	Li1			**Li2**		
O	1.7063	0.1319	-0.9933	1.9837	0.0446	-0.7221
O	-0.1824	-1.6553	-1.6402	0.0000	-1.7263	-0.1665
O	-2.0780	0.0503	-0.8175	-1.9837	0.0446	-0.7221
O	-0.1894	1.8374	-0.1705	0.0000	1.4101	0.3280
C	1.1524	2.0047	0.3090	1.2177	2.1293	0.1223
C	1.8545	0.6657	0.3259	2.2988	1.0784	0.2255
C	2.0688	-1.2512	-1.1116	2.3140	-1.2825	-0.2775
C	0.8719	-2.1174	-0.7904	1.2061	-1.8333	0.5978
C	-1.4786	-2.1674	-1.3001	-1.2061	-1.8333	0.5978
C	-2.1224	-1.2699	-0.2675	-2.3140	-1.2825	-0.2775
C	-2.3950	1.0886	0.1205	-2.2988	1.0784	0.2255
C	-1.1398	1.5133	0.8487	-1.2177	2.1293	0.1223
H	1.1564	2.4650	1.2984	1.3538	2.9014	0.8824
H	1.6424	2.6738	-0.3955	1.2152	2.5984	-0.8668
H	2.9128	0.7875	0.5679	3.2795	1.4990	-0.0002
H	1.4040	-0.0086	1.0608	2.3074	0.6672	1.2365
H	2.9131	-1.4881	-0.4621	3.2664	-1.2861	0.2546
H	2.3667	-1.3965	-2.1480	2.4143	-1.8817	-1.1805
H	1.0895	-3.1682	-0.9949	1.4068	-2.8746	0.8594
H	0.5825	-2.0194	0.2605	1.0999	-1.2505	1.5177
H	-1.4078	-3.1952	-0.9404	-1.0999	-1.2506	1.5177
H	-2.0588	-2.1528	-2.2205	-1.4067	-2.8746	0.8593
H	-3.1572	-1.5696	-0.0866	-2.4143	-1.8817	-1.1805
H	-1.5784	-1.3039	0.6815	-3.2664	-1.2861	0.2546
H	-3.1644	0.7580	0.8202	-2.3074	0.6672	1.2365
H	-2.7832	1.9175	-0.4681	-3.2795	1.4990	-0.0002
H	-1.3339	2.3862	1.4762	-1.2152	2.5984	-0.8668
H	-0.7569	0.7069	1.4818	-1.3538	2.9013	0.8824
Li	-0.2237	0.3778	-1.5869	0.0000	-0.0114	-1.0538

Table S4: continue

	Li3			**Li4**		
O	-1.6127	0.0658	-0.7166	-1.5959	0.1177	-0.8036
O	-0.0744	2.1650	-0.2335	-0.0450	2.2694	-0.5110
O	-0.1610	-0.8961	-2.7008	1.5560	0.2419	-1.1793
O	1.7025	0.6969	-1.5945	-0.1873	-0.9880	-2.7820
C	-1.5668	0.4697	0.6524	-1.5648	0.6593	0.5173
C	-1.1908	1.9368	0.6340	-1.1666	2.1161	0.3684
C	-1.3678	-1.5929	-2.3648	-1.3330	-1.6935	-2.2876
C	-1.7281	-1.3439	-0.9125	-1.6508	-1.3084	-0.8545
C	2.1236	-0.4963	-2.2695	1.7079	-1.1760	-1.2549
C	1.0276	-1.5389	-2.2271	1.0935	-1.5978	-2.5768
C	1.2304	1.9593	0.3289	1.2600	2.2117	0.0792
C	1.8236	0.6574	-0.1704	1.7938	0.7917	0.1170
H	-0.8224	-0.1320	1.1838	-1.1867	-2.7718	-2.3722
H	-2.5372	0.3285	1.1345	-2.1550	-1.3992	-2.9376
H	-2.0067	2.5239	0.2165	-0.9256	-1.7241	-0.1498
H	-0.9781	2.2972	1.6417	-2.6453	-1.6689	-0.5800
H	-1.2699	-2.6618	-2.5638	1.2030	-1.6402	-0.4035
H	-2.1341	-1.1826	-3.0194	2.7640	-1.4557	-1.2248
H	-2.7453	-1.6851	-0.7073	1.0156	-2.6851	-2.6347
H	-1.0479	-1.8594	-0.2283	1.7147	-1.2467	-3.3989
H	3.0460	-0.8832	-1.8320	1.8925	2.8247	-0.5602
H	2.3169	-0.1956	-3.2971	1.2485	2.6446	1.0812
H	1.2803	-2.3852	-2.8699	1.2825	0.1832	0.8678
H	0.8784	-1.9102	-1.2104	2.8624	0.7976	0.3464
H	1.1864	1.9677	1.4193	-0.8461	0.0994	1.1215
H	1.8442	2.7925	-0.0089	-2.5469	0.5845	0.9910
H	2.8751	0.5835	0.1185	-1.9771	2.6723	-0.0990
H	1.2858	-0.2049	0.2357	-0.9539	2.5578	1.3437
Li	-0.2506	0.9831	-1.8760	-0.1611	0.8555	-1.9518

2.3 Comparison of the computational spectra of 12c4-H$^+$ and neutral 12c4

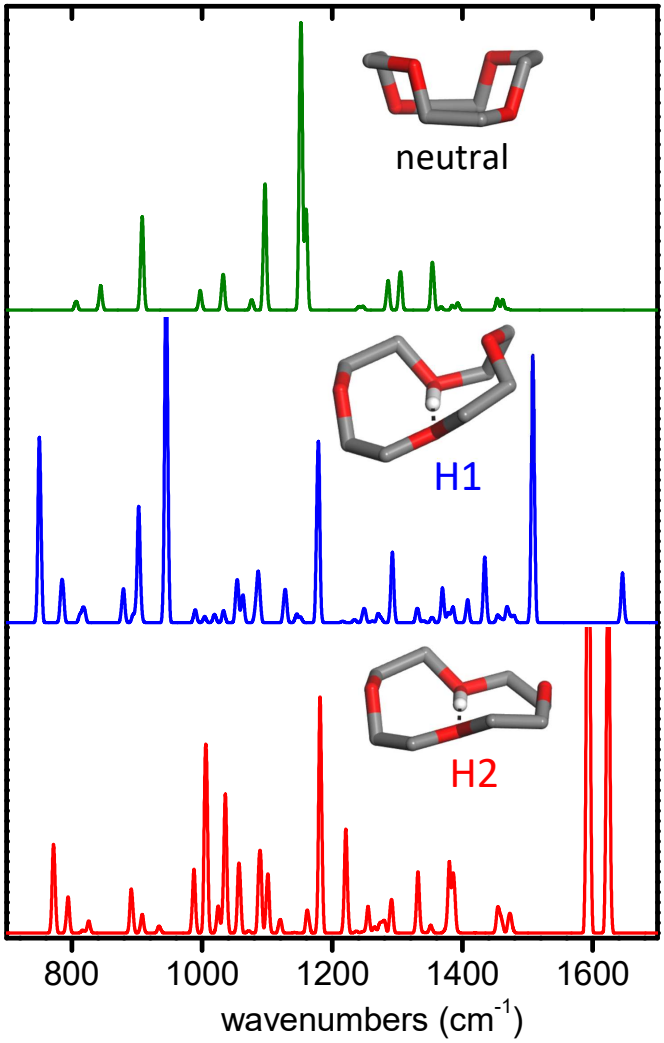

Fig. S5: Comparison of computational spectra (MP2/aug-cc-pVTZ, frequency scaling factor 0.97) for the lowest energy conformers of isolated 12-crown-4 in neutral (top) and protonated (middle and bottom) forms. The corresponding conformations are depicted in the insets (H atoms of the CH_2 groups are not shown for better visualization of the backbone configurations).

3 Comparison of Computational and Experimental Spectra

Computational spectra were generated from the MP2 and DFT calculations by convoluting the calculated stick spectra with Gaussian functions with a full width at Half-Maximum (FWHM) of 0.4% of the transition frequency. The harmonic frequencies were scaled by factors of 0.970, 0.980, 0.970, 0.965, 0.970, 0.945 for the MP2, B3LYP, ωB97xD, DSD-PBEP86, B2PLYP, and PBEQIDH computations, respectively[2]. These factors yield a good agreement for the position of the central most intense bands in the experimental spectra.

3.1 Harmonic spectra for 12c4Li+

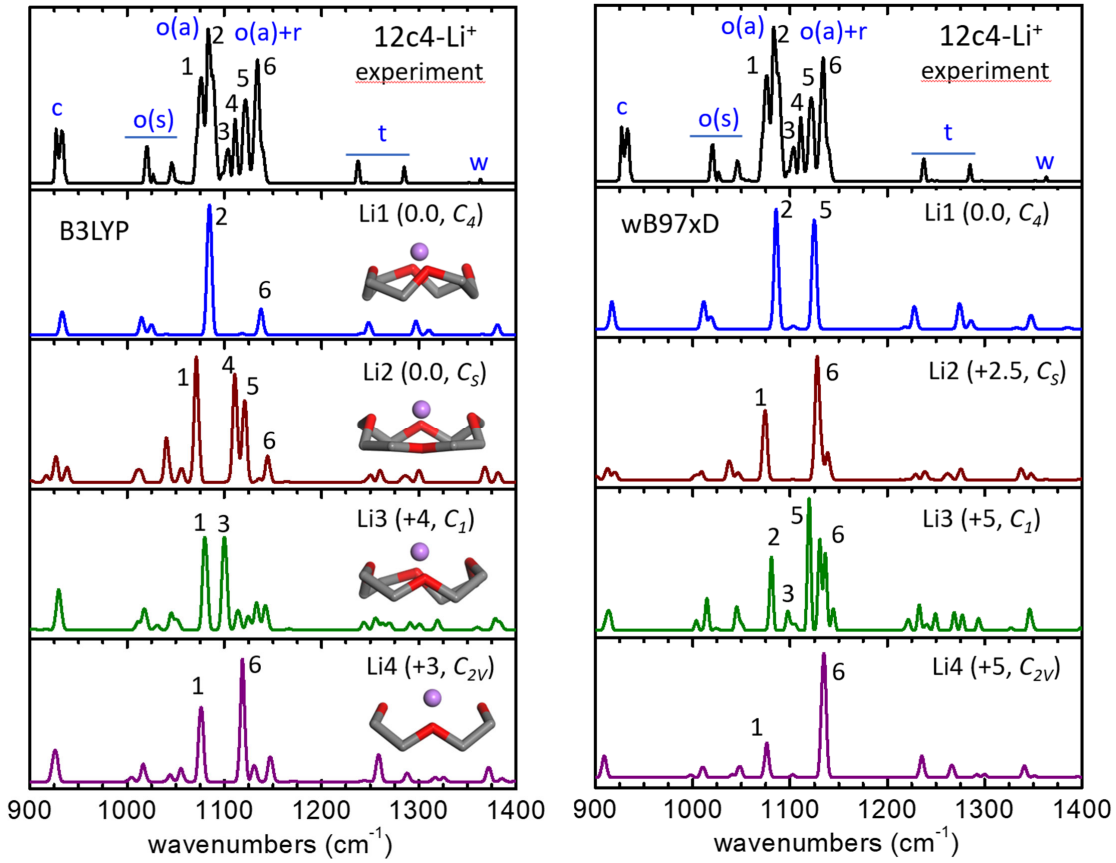

Fig. S6: He-droplet IR spectrum of the 12c4-Li^+ complex (top black trace) compared to B3LYP (left) and ωB97xD (right) harmonic spectra for the four conformers of lowest energy, Li1–Li4 (aug-cc-pVTZ basis set, D3(BJ) correction, frequencies scaled by factors 0.99 and 0.96, respectively). Side views of the conformers are inserted (H atoms of the methylene groups obviated, point symmetries and relative zero-point corrected energies in kJ·mol^{-1} are indicated). A qualitative assignment of the vibrational bands is outlined as c: C-C stretching; o(s)/o(a): symmetric/asymmetric COC stretching; r/t/w: methylene rocking, twisting and wagging. The peak numbering highlights the correlation between the experimental and computational bands.

Additionally to the MP2 calculations shown in the main text, DFT calculations using different exchange-correlation functionals (B3LYP and ωB97xD) were performed for the 12c4-Li^+ complex. The resulting computational spectra are depicted in Fig. S6 for the four conformers of the lowest energy. When averaged over the four conformers, the calculated spectra are similar to each other, and in reasonable agreement with the experimental spectrum, despite differences in the precise assignments of the intense peaks observed around 1100 cm^{-1} (peaks numbered 1–6 in Fig. S6).

3.2 Harmonic spectra for 12c4H+ and 12c4D+

MP2 frequency calculations were performed for both 12c4H+ and 12c4D+ in the harmonic approximation (Fig. 4). The MP2 spectrum for the H2 conformer of 12c4-D^+ accounts for the most salient features of the He droplet measurement. While the analogous spectrum for the H1 conformer compares less satisfactorily, its incorporation helps to reproduce the structured envelope of the most intense and congested band in the 12c4-D^+ spectrum at around 1180 cm^{-1}. The MP2 computation traces back this band to a pair of asymmetric C-O-C stretching mode components that vary slightly in frequency in the H1 and H2 conformers. The position of the higher frequency CH_2 bending modes (1300-1600 cm^{-1}) and of some of the lower frequency C-O and C-C stretching bands (<1100 cm^{-1}) are partially reproduced by the computation. The MP2 computation predicts a remarkably intense transition at frequencies slightly below 800 cm^{-1} for the two conformers, which it attributes to a symmetric C-O stretching in the ether groups participating in the proton bond. This motion couples to O-D^+ stretching in the proton bond, which in turn yields a strong transition moment of the transition. In contrast, the experiment lacks any appreciable signal in this region and it is not straightforward to assign this vibrational mode to any of the bands in the experimental spectrum.

For the 12c4-H^+ system, the differences between the computed MP2 spectra and the He-droplet spectrum are quite significant, despite a partial agreement for some of the main bands in the 1100-1500 cm^{-1} range. The mismatch of the experimental bands with the MP2 predictions becomes particularly evident in the low-frequency region (below 1100 cm^{-1}), where the experiment displays a sequence of prominent bands. In particular, the computations predict only one band below 800 cm^{-1}, where the experiment displays intense signatures (bands l, m, n, o). These modes may result from the coupling of proton motions to backbone modes, as suggested above. Fig. S7 shows that a similar situation holds for the DFT computations with the five functionals presently explored, none of which produces spectra in systematically better agreement with the experiment than the MP2 computation, and none of them yields a good agreement with the experiment.

A remarkable prediction of all computations for 12c4-H^+ is the presence of two intense transitions in the 1450-1800 cm^{-1} spectral window, that are attributed to the stretching and in-plane bending of the O–$H^+\cdots$O proton bond moiety. The relative position and intensity predicted for these two bands are sensitive to both the crown ether configuration and the level of theory employed. Fig. 4 shows that the MP2 spectrum of the H2 conformer displays two strong close-lying transitions in the 1600-1650 cm^{-1} range, whereas that of the H1 conformer features a strong transition at 1520 cm^{-1} (O-H^+ stretching) and a weaker one at 1660 cm^{-1} (in-plane

bending, *i.e.*, in the plane of the crown ether cavity). Varying intensities and band positions are predicted with other computational methods (Fig. S7). Given the limited accuracy of the computations for the spectral structure of 12c4-H^+, it is difficult to make definite assignments. Peaks α and β in the experiment may be attributed to two distinct stretching and bending vibrational modes of a single conformer or, alternatively, to a single mode with a larger transition moment (*e.g.*, O-H^+ stretching) in two different conformations of the protonated crown ether. A comparably less intense out-of-plane bending mode of the proton bond is predicted at lower frequencies. For instance, this mode lies at 1350 and 1200 cm^{-1} in the MP2 computation for the H1 and H2 conformers of 12c4-H^+, hence coinciding with bands c and d.

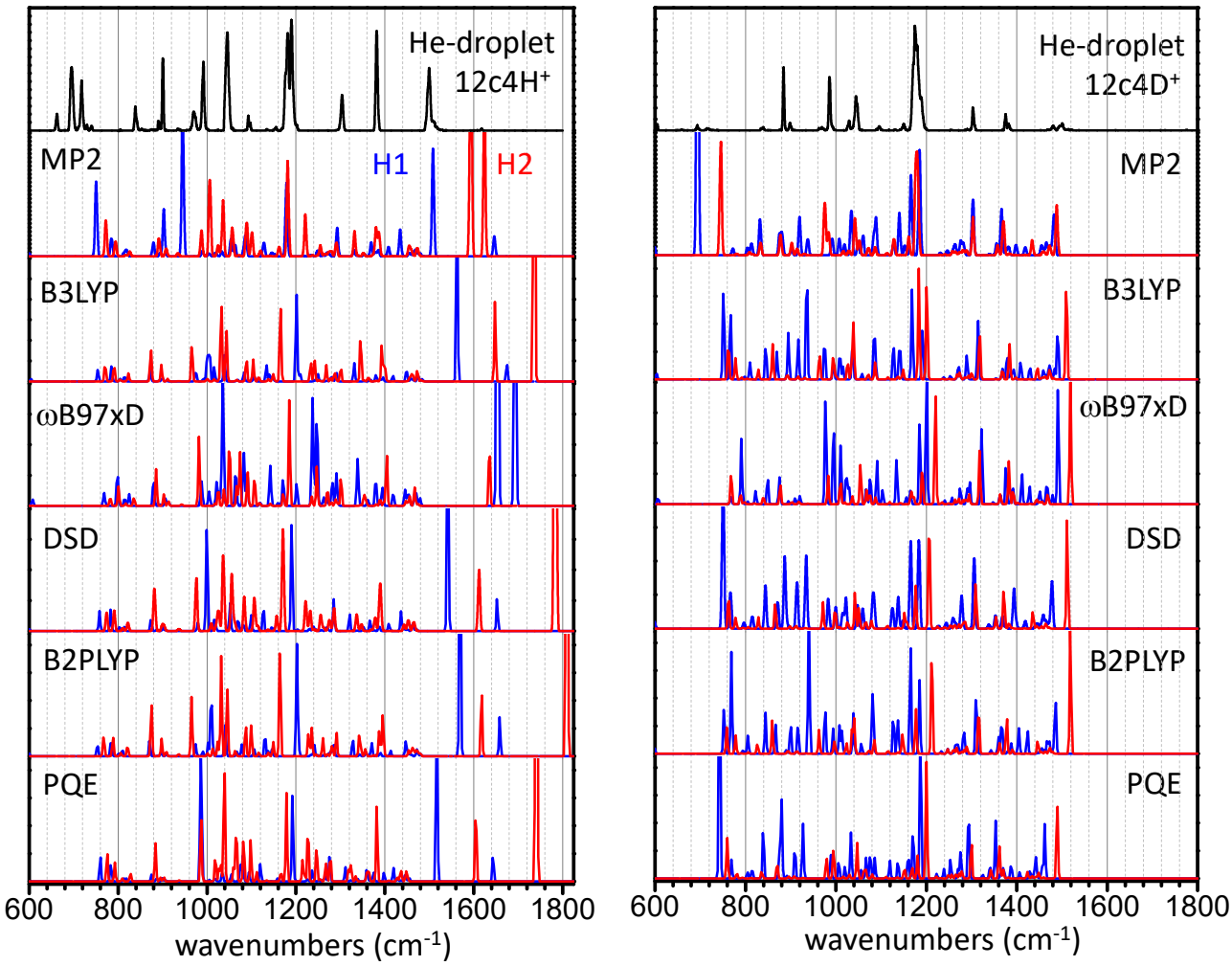

Fig. S7: Comparison of the He-droplet IR spectra of the 12c4-H^+ and 12c4-D^+ complexes (top black traces) with computations at different levels for the two conformers of lowest energy, H1 and H2 (aug-cc-pVTZ basis set, frequencies scaled respectively by factors: 0.970, 0.980, 0.970, 0.965, 0.970, 0.945).

3.3 BOMD Computations

The BOMD trajectories computed sample the actual potential electronic energy surface of the system (at a given computational level) and intrinsically incorporate anharmonic vibrational features from the Fourier Transform deconvolution of the time evolution of dipole moments of the ion. This approach leads in fact to an excellent agreement with the room-temperature IRMPD spectra of the protonated 12c4, 15c5, and 18c6 crown ethers[3].

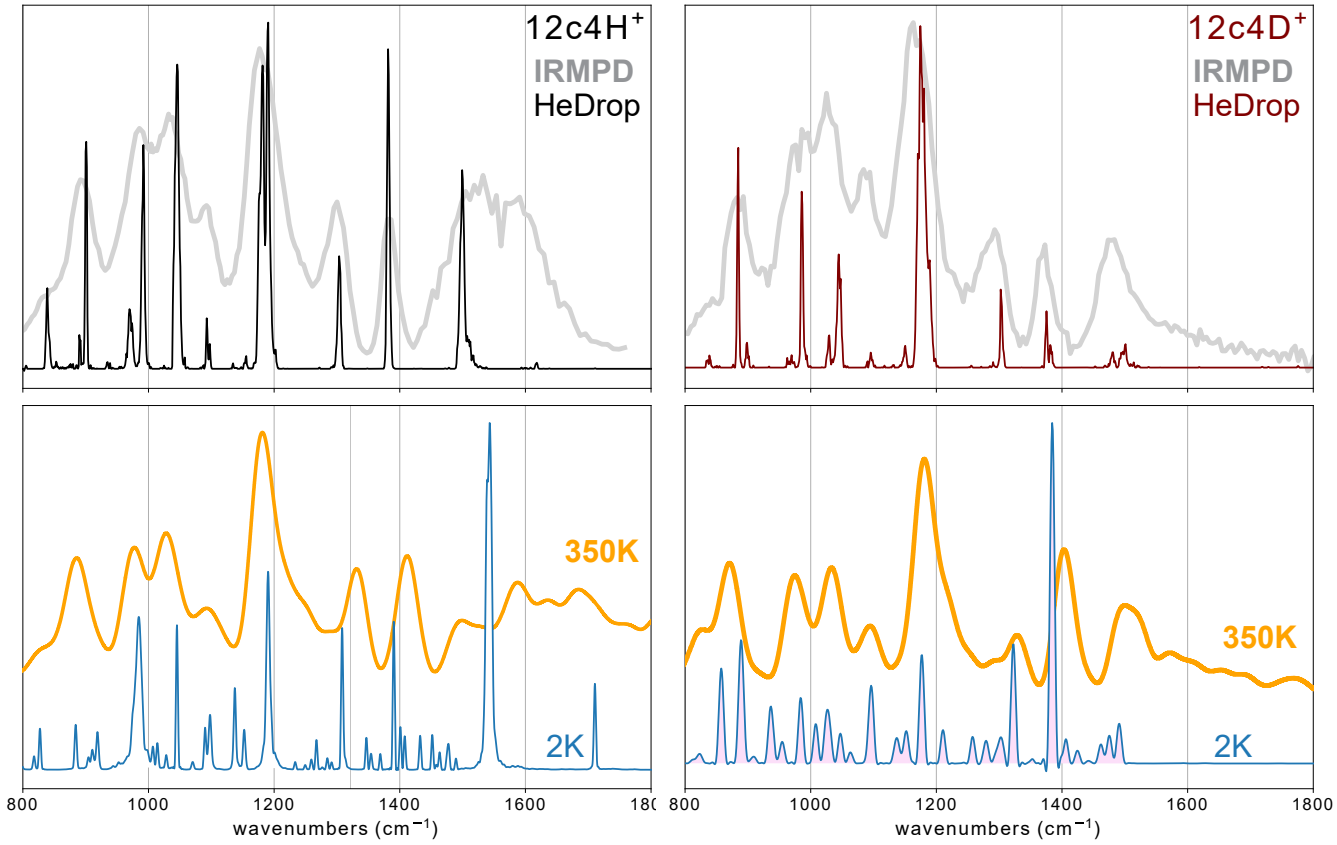

Fig. S8: Comparison of the He-droplet IR spectra of the 12c4-H^+ and 12c4-D^+ complexes (top traces) with the theoretical spectra obtained using BOMD-B3LYP at temperatures 350 K and 2 K.

Fig. S8 shows that BOMD, as applied here with the B3LYP functional, does not improve the agreement with the experiment, with respect to DFT. It must be noted that BOMD trajectories must be interpreted with caution at cryogenic temperatures as the description of proton motions and the associated mode couplings and vibrational signatures can be expected to be severely affected by the lack of nuclear quantum effects (*e.g.*, zero-point energy and tunneling) within the BOMD approach.

Details of BOMD computations: The B3LYP-D3(BJ) functional and the double-ζ DZVP basis set were employed, as implemented in the CP2K package[4]. The Goedecker-Teter-Hutter pseudopotentials were used to effectively account for the inner electrons[5]. The cut-off radius

for the pair potential was set to 12.5 Å, the plane wave cutoff to 400 Ry and the relative cutoff for the Gaussian grid to 50 Ry. The molecular system was thermally equilibrated for 5 ps in the canonical (NVT) ensemble, with the canonical sampling through velocity rescaling thermostat. Subsequently, the main production run proceeded in the microcanonical (NVE) ensemble for 150 ps. In order to probe the sensitivity of the dynamics to the PES topology, BOMD computations were performed at nominal temperatures T = 1, 2, 5, 10 K, which resulted in effective temperatures of 1.1±0.2, 2.5±0.5, 5.5±1 and 11±2 K, respectively. Additional BOMD computations at 350 K were also performed as a link with the previous IRMPD investigations[3]. Infrared spectra were produced from the BOMD trajectories with the TRAVIS analyzer package[6], based on the Fourier transform of the time correlation function of the molecular dipole moment evaluated from the maximally localized Wannier functions[7].

4 Discrete Variable Representation

Discrete variable representation[8] (DVR) was employed, as previously outlined by Colbert and Miller[9] to obtain the eigenstates and eigenvectors of the vibrational Hamiltonian for the protonated and deuterated 12-crown-4-ether. The Hamiltonian matrix was constructed and diagonalized using Python. To construct the potential energy curve, different structures were generated, as detailed below, and those energies were computed at the B3LYP/aug-cc-pVTZ level of theory, using Gaussian 16[10]. The procedure to estimate the frequency and intensity of the H1 and H2 conformations of 12c4H$^+$ and 12c4D$^+$ of the three degrees of freedom of the proton (Fig. S9) involves several steps. We employ an iterative scheme, wherein the first iteration, the B3LYP crown ether core is used. Next, the ground state DVR wave function and the expectation value for the proton location are calculated. Then, the structure is re-optimized at the B3LYP level with the O-H bond distance fixed to the DVR expectation value. This process is converged to a stable proton location after two iterations. Depending on the structure and isotope, this process caused the O-O distance to contract by 0.02 - 0.05 Å.

The optimization/calculation procedure is described as follows: First, independently for H1 and H2 equilibrium conformation, the movement of the hydrogen along the nearest oxygens was investigated ($\mathbf{x}$). The crown ether skeleton was frozen and the potential of the proton along the linear path between the two most proximal oxygen atoms was explored by calculating 100 energy points and the dipole moment. These values were used to create the 1-dimensional potential energy curve.

Next, the DVR method was employed to obtain the eigenstates and eigenvectors of the vibrational Hamiltonian, using the mass of hydrogen or deuterium as appropriate. The expectation value of the proton's position along the explored coordinate was calculated. Then, the bond length of the O-H bond was constrained to that expectation value, and the geometry of the entire complex was re-optimized (with the proton's position frozen). The resulting crown ether skeleton geometry was used as a new starting point for generating a new potential energy curve along the same coordinate, and then performing DVR to obtain a new expectation value for the O-H bond length.

The process was repeated iteratively to calculate the potential energy curve at the proton's

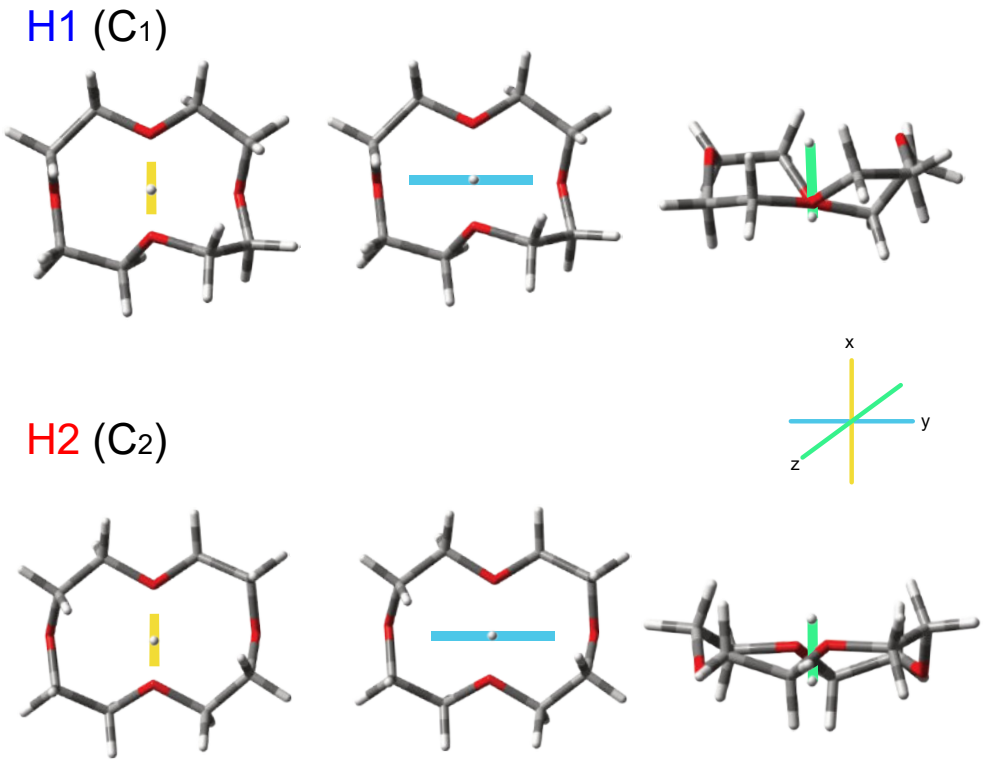

Fig. S9: Vibrational coordinates explored and calculated by DVR. **x**: the stretching coordinate of the proton along the nearest two oxygens, **y**: the perpendicular motion to the stretching, parallel to the plane of the crown ether, and **z**: the motion perpendicular to the plane of the crown ether

expected position. After two iterations, the expectation value converged (Table S5). We did the procedure described above to estimate the positions of the proton/deuteron of H1 and H2 structures. After convergence of the expectation value for this stretching coordinate, we use a similar procedure to scan the potential energy along the other two relevant modes **y** and **z** (See Fig S9). The resulting frequencies are shown in Table S6.

The transition dipole moment ($\hat{\mu}_q$, TMD) was calculated for each of the three transitions. Since the square of the TMD is proportional to the IR intensity, we estimated the IR intensity using the formula above and multiplied the result by 1000 to facilitate a better comparison of the intensities (Table S6).

$$I_{nm,IR} \propto ([\mu_x]^2_{nm} + [\mu_y]^2_{nm} + [\mu_z]^2_{nm}) \tag{1}$$

where

$$[\mu_q]^2_{nm} = \langle \Psi^*_m | \, \hat{\mu}_q \, | \Psi_n \rangle$$

Table S5. Relative electronic energies, O-H/D length, DVR-calculated frequencies, and the expectation values of O-H/D length of each iteration of H1 and H2 geometries of the stretching coordinate of 12c4-H^+ and 12c4-D^+. After each iteration, optimizations with the fixed O-H/D length were carried at the B3LYP/aug-cc-pVTZ level of theory

	H1						H2					
	12c4H^+			12c4D^+			12c4H^+			12c4D^+		
iteration	0	1	2	0	1	2	0	1	2	0	1	2
O-O (Å)	2.429	2.411	2.410	2.429	2.412	2.410	2.464	2.419	2.416	2.464	2.423	2.417
O-X (Å)	1.1150	1.1822	1.1917	1.1150	1.1734	1.1861	1.0905	1.1830	1.2010	1.0905	1.1672	1.1944
E ($kJ{\cdot}mol^{-1}$)	0.000	0.350	0.408	0.000	0.2912	0.3744	0.000	0.598	0.6474	0.000	0.5148	0.6344
$\Delta\nu$ (cm^{-1})	1352	1422	1426	866	906	909	1198	1367	1382	766	853	872
<x>(Å)	1.1822	1.1917	1.1934	1.1734	1.1861	1.1890	1.1828	1.2010	1.2010	1.1672	1.1944	1.2024

Table S6. DVR-calculated frequencies, and calculated intensities of the three proton motions of 12c4-H^+ and 12c4-D^+ in H1 and H2 geometries. The intensities were calculated proportionally to the square of the TDM as indicated in Eq. 1. The resulting number was multiplied by 1000 for a better visualization.

	H1			H2		
	12c4H^+			12c4H^+		
	x	**y**	**z**	**x**	**y**	**z**
$\Delta\nu$ (cm^{-1})	1426	1547	1309	1382	1657	1217
I (a.u.)	731.3	13.5	14.1	834.7	8.7	7.8
	12c4D^+			12c4D^+		
	x	**y**	**z**	**x**	**y**	**z**
$\Delta\nu$ (cm^{-1})	909	1167	902	872	1175	860
I (a.u.)	582.3	9.3	10.2	670.7	5.9	5.5

Based on the computation of the Transition Dipole Moment (TDM), we anticipate that the stretching motion between the nearest oxygen atoms will exhibit the greatest intensity. However, experimentally, we expect many modes to be coupled with the proton motion, making it challenging to predict the intensity of each individual vibration.

References

[1] S. Grimme, S. Ehrlich and H. Krieg, *J. Comput. Chem.*, 2011, **32**, 1456–1465.

[2] *Computational Chemistry Comparison and Benchmark Database, NIST Standard Reference Database Number 101 (Release 22, May 2022)*, (accessed september 2024), http://cccbdb.nist.gov/vibscalejust.asp.

[3] F. Gámez, J. R. Avilés-Moreno, G. Berden, J. Oomens and B. Martínez-Haya, *Phys. Chem. Chem. Phys.*, 2021, **23**, 21532–21543.

[4] T. D. Kühne, M. Iannuzzi, M.and Del Ben, V. Rybkin, P. Seewald, F. Stein, T. Laino, R. Z. Khaliullin, O. Schütt, F. Schiffmann *et al.*, *J. Chem. Phys.*, 2020, **152**, 194103 1–47.

[5] S. Goedecker, M. Teter and J. Hutter, *Phys. Rev. B*, 1996, **54**, 1703–1710.

[6] M. Brehm, M. Thomas and B. Kirchner, *J. Chem. Phys.*, 2020, **152**, 164105.

[7] M. Sharma, Y. Wu and R. Car, *Int. J. Quantum Chem.*, 2023, **95**, 821–829.

[8] J. C. Light and T. Carrington, *Advances in Chemical Physics*, John Wiley & Sons, Inc., 2000, pp. 263–310.

[9] D. T. Colbert and W. H. Miller, *J. Chem. Phys.*, 1992, **96**, 1982–1991.

[10] F. Ding, F. Lipparini, F. Egidi, J. Goings, B. Peng, A. Petrone, T. Henderson, D. Ranasinghe, V. Zakrzewski and J. Gao, *Gaussian 16, Rev/A. 03*, 2016.